Quantifying Uncertainty of Effective Transport Parameters

Zhiming Lu,[1] Hailin Deng,[2] Zhenxue Dai,[1] Andrew V. Wolfsberg,[1] Paul Reimus,[1]

Upscaling of transport parameters has been widely used in field-scale transport models to incorporate their subgrid heterogeneities. A typical practice is that single effective parameter values are used in upscaling the transport equations and uncertainties of the effective parameters are not taken into account. In this study, by taking solute transport in fractured rocks as an example, we demonstrate that the effective transport parameters may be treated as random variables and characterized by their means and variances, both of which are scale-dependent. When the dimensionless domain (or block) size is very large, the variability of the effective parameters is very small, and their mean effective parameter values may be directly applied to field-scale transport modeling. However, when the dimensionless domain size is small, the variability of the effective parameters could be very large. As a consequence, in field-scale modeling, one should take into account the variability of effective parameters. Illustrative examples show that results from transport models with variable effective parameters are superior to those with single effective parameters.

1. Introduction

It is well known that geologic formations are physically and chemically heterogeneous at various length scales. A conventional approach to modeling flow and transport in heterogeneous geological formations is to incorporate the overall heterogeneity of the system into models. This is computationally very demanding for field-scale numerical simulations. As a result, in modeling flow and transport in such field-scale heterogeneous porous media, it is quite often that the size of grid blocks in numerical models is much larger than the scale at which measurements of flow and transport parameters are taken. For example, some transport parameters are often measured at the column scale, which is much smaller than grid blocks in field-scale simulations. Therefore, one needs to assign flow and transport parameter values to numerical grid blocks based on statistics of the parameters derived from the measurement scale. The values at the grid blocks, called upscaled parameter values or effective values, should include the effect of subgrid heterogeneity and can be derived by upscaling approaches that define an equivalent homogeneous medium with upscaled (effective or macroscopic) flow and transport properties.

Many studies on the scaling of transport parameters in fractured rock have been conducted [*Berkowitz and Scher*, 1998; *Reimus et al.*, 2003; *Dai et al.*, 2007; *Liu et al.*, 2007; *Frampton and Cvetkovic*, 2007; *Dai et al.*, 2009; among others]. In a simplified fracture model, the fractures may be considered as the primary pathway for flow in fractured rocks and the matrix as a reservoir to store solutes temporarily, and exchange of solutes between fractures and matrix are through matrix diffusion and sorption. The rate of mass transfer between fractures and surrounding matrix can be described by a mass transfer coefficient [*Reimus et al.*, 2003]. This parameter includes the lumped effect of the matrix diffusion coefficient, retardation factor, fracture aperture, and matrix porosity.

Dai et al. [2009] developed a methodology to upscale matrix sorption coefficients for fractured-rock systems by assuming that the tortuosity and the retardation factor are uncorrelated random fields. The breakthrough curve (BTC) derived from the transport simulation using the upscaled effective tortuosity and effective retardation factor was compared with the BTC from a simulation with the geometric mean parameter values and the mean BTC from Monte Carlo simulations, which was consider as "true" BTC. Their results indicate that, while the BTC from effective parameter values is closer to the true BTC at the late time, large discrepancy has been observed at the early time. This implies that single effective parameter values may not be adequate to capture heterogeneities of the parameter fields and may lead to large discrepancy in predicting breakthrough curves.

In this study, based on the mass transfer coefficient between the fracture and matrix, we first derived analytical expressions for the scale-dependent mean and variance of the effective tortuosity and the effective retardation factor. Using an illustrative example, we then demonstrated that results from transport models with variable effective parameters are superior to those with single effective parameters.

2. Mathematical Development

A fracture-matrix system may be simplified as a set of parallel-plate fractures of constant aperture in surrounding matrix. Solute transport in the system may be modeled as a one-dimensional advection-dispersion process with fluid flow in fractures only and solute diffusion into the surrounding matrix in the direction perpendicular to the fracture flow [*Maloszewski and Zuber*, 1985; *Reimus et al.*, 2003].

The mass transfer between the fracture and matrix can be characterized by a mass transfer coefficient defined as [*Reimus*, 2003; *Dai et at.*, 2009]: $C_{MT} = \phi\sqrt{D_0\tau R}/b\eta$, where D_0 is the diffusion coefficient of the species of interest in free water, b is the half aperture, η and ϕ are respectively the porosity of the fracture and that of the matrix, R and τ are respectively the retardation factor and tortuosity of the matrix. It is assumed that R and τ are spatial random fields, which vary in the flow direction but are constants in the direction perpendicular to fracture flow.

Because matrix properties vary spatially, the mass transfer coefficient can also be considered as a one-dimensional random variable along the fracture. The field-scale effective mass transfer coefficient may be expressed as a volume average of the measurement-scale mass transfer coefficients [*Dai et al.*, 2009]:

$$\frac{\tilde{\phi}\sqrt{D_0\tilde{\tau}\tilde{R}}}{\tilde{\eta}\tilde{b}} = \frac{1}{L}\int_L \frac{\phi\sqrt{D_0\tau R}}{\eta b}dx, \qquad (1)$$

[1] Computational Earth Sciences Group (EES-16), Los Alamos National Laboratory, Los Alamos, NM 87545

[2] Department of Scientific Computing and Department of Geological Sciences, Florida State University, Tallahassee, FL 32306

0094-8276/09/$5.00

where L is the length of the one-dimensional domain (along the fracture), and the tilde above each variable denotes the effective quantity. By assuming ϕ, η, and b are deterministic constants, this equation can be rewritten as:

$$\tilde{\tau}\tilde{R} = \left[\frac{1}{L}\int_L \sqrt{\tau R}dx\right]^2. \quad (2)$$

We further assume that τ and R are two log-normally distributed, second-order stationary random fields, and decompose them formally as $Y = \ln(R) = \langle Y\rangle + Y'(x)$ and $Z = \ln(\tau) = \langle Z\rangle + Z'(x)$, where $\langle Y\rangle$ and $\langle Z\rangle$ are means of Y and Z, and $Y'(x)$ and $Z'(x)$ are their zero-mean perturbations. Substituting these decompositions into (2) yields

$$\tilde{\tau}\tilde{R} = \frac{\tau_G R_G}{L^2}\int_L\int_L e^{\left(\frac{1}{2}[Y'(x)+Y'(y)+Z'(x)+Z'(y)]\right)}dxdy, \quad (3)$$

where $\tau_G = \exp(\langle Y\rangle)$ and $R_G = \exp(\langle Z\rangle)$ are geometric means of τ and R, respectively.

Our purpose is to find individually the moments of effective tortuosity $\tilde{\tau}$ and effective retardation factor $\tilde{R}$. Because these two effective parameters appear in (3) as their product, we will derive moments of $\tilde{\tau}$ and $\tilde{R}$ by first finding those of $\tilde{\tau}\tilde{R}$. For convenience, we denote $w = \tilde{\tau}\tilde{R}$ and write $w = w^{(0)} + w^{(1)} + w^{(2)} + \cdots$, where numbers in parentheses represent the order in terms of standard deviations of input parameters. Expanding the right side of (3) up to second order and separating terms at different orders yield

$$w^{(0)} = \tau_G R_G, \quad (4)$$

$$w^{(1)} = \frac{\tau_G R_G}{L}\int_L [Y'(x) + Z'(x)]dx, \quad (5)$$

$$w^{(2)} = \frac{\tau_G R_G}{4L}\left[\int_L [Y'(x) + Z'(x)]^2 dx + \frac{1}{L}\int_L\int_L [Y'(x) + Z'(x)][Y'(y) + Z'(y)]dxdy\right]. \quad (6)$$

From (4)-(6) it is seen that the moments of w depend on the auto-correlation of τ and R and the possible cross-correlation between these two random fields. To evaluate the moments of w, we have to assume these correlation structures. For simplicity, we assume that these two random are correlated and they have the same correlation structures. Otherwise, we need to find the square roots of their covariances [*Oliver*, 2003], which complicates the problem.

The mean of w up to second order $\langle w\rangle \approx w^{(0)} + \langle w^{(2)}\rangle$ can be obtained by taking expectation of (4)-(6) and carrying out integrals:

$$\langle w\rangle \approx \tau_G R_G\left[1 + \frac{1}{4}\left[\sigma_Y^2 + \sigma_Z^2 + 2\rho_{YZ}\sigma_Y\sigma_Z\right](1+\gamma(l))\right], \quad (7)$$

where σ_Y^2 and σ_Z^2 are variances of $Y = \ln R$ and $Z = \ln\tau$, respectively, ρ_{YZ} is their cross-correlation coefficient, $l = L/\lambda$ is the dimensionless domain size, and $\gamma(l) = (1/l^2)\int_0^l\int_0^l \rho(x-y)dxdy$ is called the variance function [*Vanmarcke*, 1983; *Li et al.*, 2009], which measures the reduction of the point variance under the average over a segment of dimensionless length l. The variance function may be derived analytically for some special cases [*Li et al.*, 2009]. For example, for the exponential correlation function $\rho(x, y) = \exp(-|x - y|/\lambda)$, we have $\gamma(l) = 2(l - 1 + e^{-l})/l^2$. One important feature of the variance function is that $\gamma(l)$ is a monotonic decrease function of l satisfying $0 \le \gamma(l) \le 1$ with $\gamma(0) = 1$ and $\gamma(\infty) = 0$.

The variance of w up to second order can be derived from (5) as

$$\sigma_w^2 = \tau_G^2 R_G^2\left[\sigma_Y^2 + \sigma_Z^2 + 2\rho_{YZ}\sigma_Y\sigma_Z\right]\gamma(l). \quad (8)$$

Equations (7)-(8) will be used to derive the moments of the effective tortuosity and retardation factor.

2.1. Moments of Effective Tortuosity $\tilde{\tau}$

Equations (7)-(8) give the mean and variance of the product of the effective tortuosity and the effective retardation factor. The mean and variance for each of these two effective parameters may be estimated by assuming that the change of tortuosity due to transport processes can be negligible. Under this assumption, the statistics of the tortuosity can be obtained by considering transport of conservative solutes, and thus the perturbation, mean, and variance of tortuosity can be derived directly from (5), (7), and (8) by setting $R \equiv 1$, $\sigma_Y^2 = 0$, and $\rho_{YZ} = 0$:

$$\tilde{\tau}' = \frac{\tau_G}{L}\int_L Z'(x)dx, \quad (9)$$

$$\langle\tilde{\tau}\rangle = \tau_G\left[1 + \frac{\sigma_Z^2}{4}(1 + \gamma(l))\right], \quad (10)$$

$$\sigma_{\tilde{\tau}}^2 = \tau_G^2\sigma_Z^2\gamma(l). \quad (11)$$

Equations (10)-(11) indicate that the mean and variance of the effective tortuosity depend on the scale $l = L/\lambda$. Because the range of the variance function $\gamma(l)$ is between zero and one, the effective tortuosity is always larger than its geometric mean, and the range of the mean effective tortuosity is $\tau_G\exp(\sigma_Z^2/4) \le \langle\tilde{\tau}\rangle \le \tau_G\exp(\sigma_Z^2/2) = \tilde{\tau}_A$, where the upper bound is its arithmetic mean. In addition, the variance of the effective tortuosity $\sigma_{\tilde{\tau}}^2$ is always smaller than the variance of tortuosity $\sigma_\tau^2 = \tau_G^2 e^{\sigma_Z^2}(e^{\sigma_Z^2} - 1)$. When l is very small, $\gamma(l)$ approaches one and $\sigma_{\tilde{\tau}}^2 \approx \tau_G^2\sigma_Z^2$, which is the first-order approximation of σ_τ^2.

To illustrate the characteristics of the effective tortuosity, we use the example in *Dai et al.* [2009]. The mean and variance of log tortuosity are $\langle Z\rangle = -3.615$ ($\tau_G = 0.0269$) and $\sigma_Z^2 = 0.4$, respectively. The calculated mean and variance of the effective tortuosity using (10)-(11) as functions of l are plotted in Figure 1(a). Also plotted in the figure is the confidence interval denoted as upper and lower bounds, which are computed from plus and minus two standard deviations of the log mean effective tortuosity.

First, it is important to note from the figure that the mean effective tortuosity is scale-dependent; it decreases with the increase of l. In other words, for a fixed correlation length, a larger domain (larger l) will lead to smaller mean effective tortuosity. Second, the range of the mean effective tortuosity depends on the variability. In fact, the ratio of the maximum mean effective tortuosity to its minimum is $\exp(\sigma_Z^2/4)$. Third, as mentioned before, the mean effective tortuosity is always larger than the geometric mean, and the ratio between the maximum mean effective tortuosity and the geometric mean is $\exp(\sigma_Z^2/2)$, which is 1.20 in this example. More importantly, the variance of the effective tortuosity decreases with l. The variance approaches zero when l is sufficiently large. This implies that, if the domain is very large comparing to the correlation length λ, one single value of the effective tortuosity may be used. On the other hand, if the domain size is very small, the variance of the effective tortuosity becomes $\tau_G^2\sigma_Z^2$, which is the first-order approximation of the variance of the tortuosity at the measurement scale, $\sigma_\tau^2 = \tau_G^2 e^{\sigma_Z^2}(e^{\sigma_Z^2} - 1)$. In this case, one should not use

a single effective tortuosity value to represent the randomly heterogeneous tortuosity field. Instead, one should sample the effective tortuosity values based on the statistics of the effective tortuosity given in (10)-(11) and use these values in transport modeling.

2.2. Moments of Effective Retardation Factor $\tilde{R}$

The moments of $\tilde{R}$ can be derived from moments of $\tilde{\tau}$ and $w = \tilde{\tau}\tilde{R}$. Expanding $w = \tilde{\tau}\tilde{R} = (\langle\tilde{\tau}\rangle + \tilde{\tau}')(\langle\tilde{R}\rangle + \tilde{R}')$ and taking its expectation yield

$$\langle w\rangle = \langle\tilde{\tau}\rangle\langle\tilde{R}\rangle + C_{\tilde{\tau}\tilde{R}}, \tag{12}$$

where $C_{\tilde{\tau}\tilde{R}} = \langle\tilde{\tau}'\tilde{R}'\rangle$ is the one-point cross-covariance between $\tilde{\tau}$ and $\tilde{R}$. In *Dai et al.* [2009], it was assumed that $\tilde{\tau}$ and $\tilde{R}$ were uncorrelated, i.e., $C_{\tilde{\tau}\tilde{R}} = 0$, and $\langle\tilde{R}\rangle$ was computed directly from (12) as $\langle w\rangle/\langle\tilde{\tau}\rangle$. However, these two effective parameters may be correlated even if τ and R at the measurement scale are assumed to be uncorrelated, because these two effective parameters appear as their product in (3). To evaluate $\langle\tilde{R}\rangle$, one has to find the one-point cross-covariance $C_{\tilde{\tau}\tilde{R}}$ first.

Subtracting (12) from w yields its perturbation

$$w' = \langle\tilde{R}\rangle\tilde{\tau}' + \langle\tilde{\tau}\rangle\tilde{R}' + \tilde{\tau}'\tilde{R}' - C_{\tilde{\tau}\tilde{R}}. \tag{13}$$

To solving for $\langle\tilde{R}\rangle$, we multiply $\tilde{\tau}'$ to (13), take expectation, and ignore a third-order term:

$$C_{w\tilde{\tau}} = \langle\tilde{R}\rangle\sigma_{\tilde{\tau}}^2 + \langle\tilde{\tau}\rangle C_{\tilde{\tau}\tilde{R}}, \tag{14}$$

where $C_{w\tilde{\tau}}$ can be found using (5) and (9):

$$C_{w\tilde{\tau}} = \tau_G^2 R_G \left[\sigma_Z^2 + \rho_{YZ}\sigma_Y\sigma_Z\right]\gamma(l). \tag{15}$$

Equations (12) and (14) has two unknowns $\langle\tilde{R}\rangle$ and $C_{\tilde{\tau}\tilde{R}}$, from which we can solve for $\langle\tilde{R}\rangle$ and $C_{\tilde{\tau}\tilde{R}}$:

$$\langle\tilde{R}\rangle = \frac{\langle\tilde{\tau}\rangle\langle w\rangle - C_{w\tilde{\tau}}}{\langle\tilde{\tau}\rangle^2 - \sigma_{\tilde{\tau}}^2}. \tag{16}$$

$$C_{\tilde{\tau}\tilde{R}} = \langle w\rangle - \langle\tilde{\tau}\rangle\langle\tilde{R}\rangle. \tag{17}$$

The variance $\sigma_{\tilde{R}}^2$ can be derived by first relating it to σ_w^2 using (13):

$$\sigma_w^2 = \langle\tilde{R}\rangle^2\sigma_{\tilde{\tau}}^2 + \langle\tilde{\tau}\rangle^2\sigma_{\tilde{R}}^2 + 2\langle\tilde{\tau}\rangle\langle\tilde{R}\rangle C_{\tilde{\tau}\tilde{R}}, \tag{18}$$

and then substituting $C_{\tilde{\tau}\tilde{R}}$ in (17) into (18):

$$\sigma_{\tilde{R}}^2 = \frac{\sigma_w^2 + \langle\tilde{R}\rangle^2\sigma_{\tilde{\tau}}^2 - 2\langle\tilde{R}\rangle C_{w\tilde{\tau}}}{\langle\tilde{\tau}\rangle^2}. \tag{19}$$

Equations (16) and (19) will be used to evaluate the mean and variance of the effective retardation factor $\tilde{R}$. For statistics of tortuosity given previously and $\langle Y\rangle = 3.919$ ($R_G = 50.375$) and $\sigma_Y^2 = 0.6$, the mean effective retardation factor as a function of l at three different levels of correlation $\rho_{YZ} = -1$, 0, and 1 is illustrated in Figure 1(b).

Several important points can be made from this figure. First, unlike the mean effective tortuosity, the mean effective retardation factor can be smaller than its geometric mean when the tortuosity and retardation factor are negatively, perfectly correlated. However, when they are positively perfectly correlation, the mean effective retardation factor can be much larger than R_G. Such a difference on the effective retardation factor may lead to substantial difference in transport simulations. Second, for all three different levels of correlation, the mean effective retardation factor is scale-dependent and a large scale will lead to a small mean effective retardation factor. Third, the figure also shows that the standard deviation of the effective retardation factor is strongly dependent on l. When l is large, the variability of $\tilde{R}$ is very small, which means that one may use one effective value in transport simulations. However, when l is small, the variability of $\tilde{R}$ could be very large, which prevent us from using a single effective value to approximate the heterogeneous retardation factor.

In addition, such a scale effect depends on ρ_{YZ}. When $\ln R$ and $\ln\tau$ are highly, negatively correlated, the mean retardation factor strongly depends on the scale (solid curve with squares), while when they are highly, positively correlated, the scale effect on the mean retardation factor is relatively small (solid curve with cycles). Furthermore, although the mean and variance of the tortuosity and retardation factor are the same in all three cases, the mean effective retardation factor can be significantly different from each other. More importantly, for any fixed ρ_{YZ}, it is noted that the mean retardation factor is almost a constant if the dimensionless domain size in larger than about 100, which may be defined as a critical domain size. Existing of such a critical value can also be determined from the variance of the effective retardation factor $\tilde{R}$. When the dimensionless domain is large than 100, $\sigma_{\tilde{R}}^2$ is almost zero, and it increases as the dimensionless domain becomes smaller. The figure indicates that $\sigma_{\tilde{R}}^2$ is large if the tortuosity and the retardation factor are strongly, negatively correlated, although in this case the mean retardation factor is much smaller than those in other two cases.

3. Illustrative Example

We considered the same case as illustrated in *Dai et al.* [2009] and conducted two sets of Monte Carlo simulations to assess the accuracy of moments of the effective tortuosity and the effective retardation factor, and more importantly, to verify our concept that using multiple samples of effective parameters from their statistics rather than one single effective parameter value in transport modeling would improve simulation results.

The solute transport in the fracture-matrix system was solved using the generalized double porosity model (GDPM) [*Zyvoloski et al.*, 2008]. The GDPM numerical model has a fracture length of 1000 m, fracture spacing of 2 m, and half aperture of 0.001 m. The fracture is discretized uniformly into 1000 element (1001 nodes) with $\delta x = 1m$ and each fracture node is connected to 10 matrix nodes arranged in a line perpendicular to the fracture direction with a variable spatial spacing from 0.001 to 0.4 m (Fig. 1 of *Dai et al.*, 2009). At the inlet, the water was injected at a constant rate of 0.012 kg/s and the solute concentration was fixed at a unit.

In the first set of Monte Carlo simulations, for each simulation, two random fields $Y(x)$ and $Z(x)$ with parameter statistics given above were generated using the random field generator described in *Zhang and Lu* [2004]. The generated fields were then converted to heterogeneous fields of matrix diffusion coefficients $D_m(x) = D_0\exp(Z(x))$ and of sorption coefficients $K_d(x) = \phi(e^{Y(x)} - 1)/\rho_m$, where $D_0 = 6.64\times10^{-10}$ m^2/s is the molecular diffusion coefficient of uranium in free water, $\rho_m = 2500$ kg/m^2 is the matrix density, and $\phi = 0.2$ is matrix porosity. Transport equations (Eqn. (1) and (2) of *Dai et al.*, 2009) were then solved for each realization using the GDPM model of *Zyvoloski et al.* [2008] and the concentration breakthrough at the outflow fracture node was recorded. Total of 10,000 Monte

Carlo simulations were conducted and it has been shown that the number of realizations is large enough to ensure the convergence of the Monte Carlo simulations. The mean breakthrough curve (BTC) computed from this set of Monte Carlo simulations is considered as the "true" solutions to the problem.

In *Dai et al.* [2009], they compared three BTC's: the mean BTC calculated from Monte Carlo simulations, the one derived using geometric means of the tortuosity and the retardation factor, and the one from the effective tortuosity and the effective retardation factor which were computed by assuming that the effective tortuosity and the effective retardation factor were uncorrelated. Their results indicate that, at the later time, the BTC simulated using the effective parameter values matches the Monte Carlo results much better than the BTC from the geometric mean values does. However, at the early time, large deviations are observed between the true BTC from Monte Carlo simulations and the BTC from the effective parameter values, and the BTC from the geometric parameter values is closer to Monte Carlo results.

Our hypothesis is that single effective parameter values may not be adequate to characterize the transport process in such a heterogeneous fracture-matrix system unless the domain is sufficient large comparing to the correlation lengths of the tortuosity and/or the retardation factor. If the domain is not large enough, the uncertainties associated with the effective parameters may not be neglected as illustrated in Figures 1, and therefore one should take these uncertainties into account.

To test our hypothesis, the mean and variance of $\tilde{R}$ and $\tilde{\tau}$ were calculated using equations (10)-(11) and (16)-(19): $\langle\tilde{\tau}\rangle = 0.0305$, $\sigma^2_{\tilde{\tau}} = 9.3\times10^{-5}$, $\langle\tilde{R}\rangle = 60.92$, and $\sigma^2_{\tilde{R}} = 517.3$. Based on these statistics of the effective parameters, we conducted the second set of Monte Carlo simulations by generating 5000 sets of effective tortuosity and effective retardation factor, solving transport equations, and computing the mean BTC from all these realizations. This BTC is plotted in Figure 2, together with other three BTC's described above. The figure shows that the BTC derived from Monte Carlo samples of the effective parameters fits the BTC of the Monte Carlo simulations with spatially variable transport parameters very well, and outperforms both BTC's from the geometric mean values and from single effective parameter values.

It appears that in our upscaling procedure the original Monte Carlo simulations are replaced by another set of Monte Carlo simulations. However, in the original Monte Carlo simulations both the tortuosity and retardation factor vary not only in probability space but also on the real space, while in the second set of Monte Carlo simulations the effective parameters are random constants. One of the advantages is that the numerical transport simulations with homogeneous parameters will be computationally more efficient, and in some cases, even analytical solutions may be available.

4. Conclusion and Discussion

Transport parameters are commonly obtained from measurements at the column scale, which is much smaller than the numerical grid size in field-scale simulations. Therefore, one needs to assign transport parameter values to numerical grid blocks based on statistics of the parameters calculated from the measurement scale. The values at the grid blocks, called upscaled parameter values or effective values, should include the effect of subgrid heterogeneity and can be derived by upscaling approaches that define an equivalent homogeneous medium with upscaled (effective or macroscopic) transport properties. A typical practice is that single effective parameter values are used in upscaling the transport equations and uncertainties of the effective parameters are not taken into account.

In this study, by taking the upscaling of tortuosity and retardation factor for a fracture-matrix system as an example, we demonstrated that uncertainty of effective parameters should not be ignored when the dimensionless domain size is relatively small. We first derived analytical expressions for the mean and variance of effective transport parameters (tortuosity and retardation factor) based on the transport equations for the fracture-matrix system. Our numerical results show that both the mean and variance of the effective tortuosity and retardation factor are scale dependent. The means of both effective parameters are larger than their geometric means, and the difference depends on the scale. More importantly, the variance of the effective parameters can be very large when the scale is small, and it can be negligible only when the scale is large enough.

Acknowledgments. This work is supported by Los Alamos National Laboratory through a Laboratory Directed Research and Development (LDRD) project (20070441ER).

References

Berkowitz, B., and H. Scher (1998), Theory of anomalous chemical transport in random fracture networks, *Phys. Rev. E*, 57, 5858- 5869.

Dai, Z., A. V. Wolfsberg, Z. Lu, and P. Reimus (2007), Upscaling matrix diffusion coefficients for heterogeneous fractured rocks, *Geophys. Res. Lett.*, 34, L07408, doi:10.1029/2007GL029332.

Dai, Z., A. V. Wolfsberg, Z. Lu, and H. Deng (2009), Scale dependence of sorption coefficients for contaminants transport in saturated fractured rocks, *Geophy. Res. Lett.*, 36, L01403, doi:10.1029/2008GL036516.

Frampton, A., and V. Cvetkovic (2007), Upscaling particle transport in discrete fracture networks: 2. Reactive tracers, *Water Resour. Res.*, 43, W10429, doi:10.1029/2006WR005336.

Li, C., Z. Lu, T. Ma, and X. Zhu (2009), A simple kriging method incorporating multiscale measurements in geochemical surveys, *J. Geochem. Explor.*, 101, 147-154.

Liu, H. H., Y. Q. Zhang, Q. Zhou, and F. J. Molz (2007), An interpretation of potential scale dependence of the effective matrix diffusion coefficient, *J. Contam. Hydrol.*, 90, 41- 57.

Maloszewski, P., and A. Zuber (1985), On the theory of tracer experiments in fissured rocks with a porous matrix, *J. Hydrol.*, 79, 333-358.

Oliver, D., Gaussian cosimulation: Modelling of cross-covariance, *Math. Geol.*, 35, 6, 681-698, 2003.

Reimus, P., G. Pohll, T. Mihevc, J. Chapman,M. Haga, B. Lyles, S. Kosinski, R. Niswonger, and P. Sanders (2003), Testing and parameterizing a conceptual model for solute transport in a fractured granite using multiple tracers in a forced-gradient test, *Water Resour. Res.*, 39(12), 1356, doi:10.1029/2002WR001597.

Vanmarcke, E., 1983. *Random fields: Analysis and Synthesis.* The MIT Press.

Zhang, D. and Z. Lu (2004), An efficient, higher-order perturbation approach for flow in randomly heterogeneous porous media via Karhunen-Loeve decomposition, *J. Comput. Phys.*, 194(2), 773-794.

Zyvoloski, G. A., B. A. Robinson, and H. S. Viswanathan (2008), Generalized double porosity: A numerical method for representing spatially variable sub-grid scale processes, *Adv. Water Resour.*, 31, 535- 544.

Zhiming Lu, Computational Earth Sciences Group (EES-16), Los Alamos National Laboratory, Los Alamos, NM 87545, USA. (zhiming@lanl.gov)

Figure caption

Figure 1. Scale dependence of the mean and standard deviation of (a) the effective tortuosity, and (b) the effective retardation factor with different levels of correlation between tortuosity and retardation factor.

Figure 2. Comparison of BTC's from different modeling approaches: Conventional Monte Carlo simulations (solid cycles), geometric mean values (dashed line), single effective parameter values (dashed-dotted line), and Monte Carlo simulations of effective parameters (solid line).

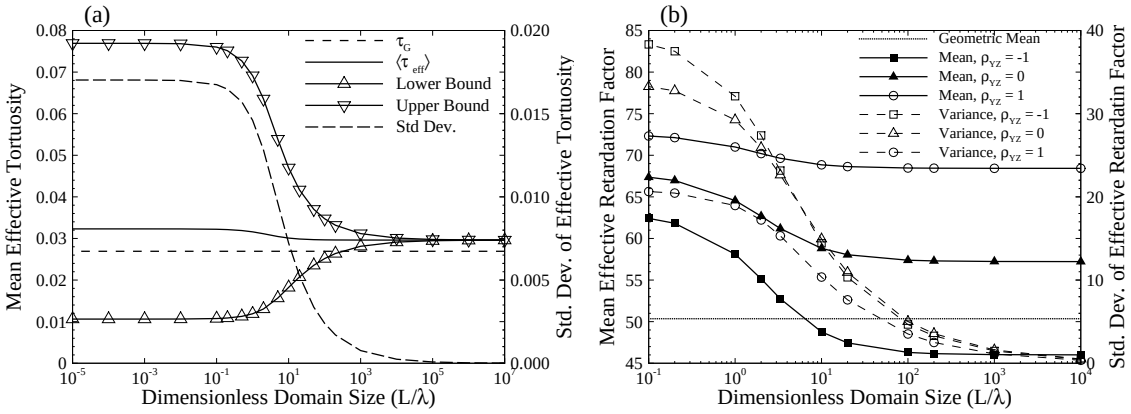

Figure 1. Scale dependence of the mean and standard deviation of (a) the effective tortuosity, and (b) the effective retardation factor with different levels of correlation between tortuosity and retardation factor.

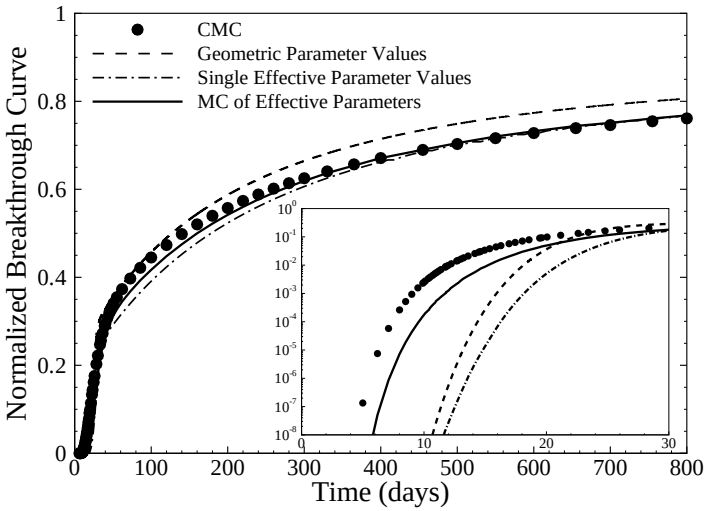

Figure 2. Comparison of BTC's from different modeling approaches: Conventional Monte Carlo simulations (solid cycles), geometric mean values (dashed line), single effective parameter values (dashed-dotted line), and Monte Carlo simulations of effective parameters (solid line).